Co_3O_4 Nanocrystals with Predominantly Exposed Facets: Synthesis, Environmental and Energy Applications

Hongqi Sun*, Ha Ming Ang, Moses O Tadé, Shaobin Wang*

Department of Chemical Engineering, Curtin University, GPO Box U1987, WA 6845, Australia.

*Correspondence Author Email: shaobin.wang@curtin.edu.au (S. Wang); h.sun@curtin.edu.au (H. Sun)

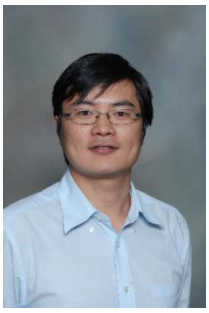

Dr. Hongqi Sun received his PhD in Chemical Engineering (2008) from Nanjing University of Technology, China. He currently works as an independent research fellow at the Department of Chemical Engineering, Curtin University, Australia. His research interests include visible light photocatalysis, solar fuels, solar cells and environmental remediation using nanostructured metal oxides and emerging nanocarbons. He has published more than 50 refereed journal papers with over 500 citations.

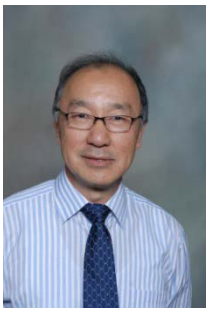

Prof. Ha Ming Ang obtained his PhD from University College London in the 1970s. His research interests include development, characterisation and application of nanostructured materials for use as photocatalysts for treatment of contaminants present in both liquids and gases. He has published over 100 refereed papers in reputed international journals.

Prof. Moses Tadé received his PhD in Chemical Engineering at Queen's University, Kingston, Ontario, Canada in 1986. At Curtin University, he became the Professor and Head of Chemical Engineering from 2001 to 2007 and after this he was promoted to Dean of Engineering in 2008. His current research interests focus on fuel cells - SOFC multiscale modelling, optimization and control, and nanostructured materials for energy and environmental applications. He has published 4 books on various aspects of his work as well as over 200 research papers. He is the founding Editor-in-Chief of Asia-Pacific Journal of Chemical Engineering (www.apjChemEng.com) and a Vice-President of IChemE worldwide.

Prof. Shaobin Wang obtained his PhD in Chemical Engineering from University of Queensland, Australia. His research interests focus on nanomaterial synthesis and application for adsorption and catalysis, fuel and energy conversion and environmental remediation. He has published more than 180 refereed journal papers and was awarded 2012 Thomson Reuters Citation & Innovation Award in Australia. He is the Editor-in-Chief of Current Catalysis and Recent Patents on Catalysis and editorial board members of several other international journals.

Abstract

Facet-dependent properties of novel metal or metal-oxide nanocrystals have been discovered recently, and attract intensive interests owing to their great potentials for various practical applications. Co_3O_4 as one of important transition metal oxides shows electronic, magnetic, and redox properties which have found many applications in energy conversion and storage, magnetic separation, sensor device and catalysis. This review summarizes the most recent research advances in synthesis and applications of nanosized Co_3O_4 with predominantly exposed facets, with emphasises on the enhanced performances in catalysis and electrochemical properties. The mechanism for improved selectivity and activity was discussed, and panorama of the correlations among particle shape, crystal plane, surface atom arrangement, and active sites has been drawn. Insightful findings in this scope may be achieved by forthcoming research in theoretical calculations, rational synthesis, and emerging applications. Thus, researchers can manipulate the synthesis at atomic level and novel applications of the materials in broad areas.

Keywords: Tricobalt tetraoxide, crystal plane, facet, energy storage, catalysis

1. Introduction

Metal oxides have dramatically facilitated the vast success in a broad range of scientific fundamentals and technological applications.[1-4] Tricobalt tetraoxide (Co_3O_4), a magnetic *p*-type semiconductor, has been demonstrated prevailing applications in heterogeneous catalysis,[5-8] energy storage and conversion,[5, 9-13] sensors and devices,[10, 14-16] etc. The performances of Co_3O_4 in such applications, corresponding to its intrinsically electronic, magnetic, optical and catalytic properties, strongly depend on both crystalline structures and surface features. The crystalline structure of Co_3O_4 has been indexed as normal spinel, based on a cubic close packing array of oxide ions. Co(II) ions are located at the tetrahedral 8a sites and Co(III) ions occupy the octahedral 16d sites.[17] On the other hand, the nature of surface, on which many physical and chemical processes take place,[18] is controlled by the size, shape, and morphology via adjusting the atomic arrangement and coordination.[19]

Nanosized Co_3O_4 crystallite is able to provide more promising properties than a conventional bulk counterpart by the manipulated high surface-to-volume ratio and more defects.[20, 21] Employing nanoparticles as building blocks offers a powerful tool to succeed in fabrication of desired 1-3 D (dimensional) nanoarchitectures of Co_3O_4.[9, 22, 23] Its nanostructures with a great variety of morphologies, such as nanocubes,[24, 25] nanorods,[7, 26] nanowires,[27, 28] nanotubes,[10, 29] nanobelts,[30, 31] nanospheres,[14, 32] nanosheets,[33, 34] nanomeshs,[35] nano-octahedra,[36] and nanocapsules,[37] etc., have been fabricated. Further investigations discovered that there is a close correlation between shape/morphology and performances of Co_3O_4 nanocrystals in practical applications.[7, 14, 24, 38-40] Rational synthesis of preferential morphology and insights to the mechanism of shape-performance correlation would be definitely desirable for better applications of Co_3O_4 in environmental remediation and energy conversion.

The nature of size or shape-related properties lies in the arrangement of surface atoms and surface energy, leading to genuine facet-dependent properties of nanomaterials.[41-45] Some reports summarized the research advances in the facet-related properties of noble metals (Pt, Pd, Au and Ag),[43, 44, 46] metal oxides (TiO_2[19, 47-50], ZnO[18, 51] and SnO_2[18, 46, 52]), and metal sulfides (CdS, Ag_2S and PbS).[53] However, the enhanced performances via preferential facets of nanocrystalline Co_3O_4 have not yet been reported.[43, 54]

This review therefore provides very recent advances in the design and synthesis of nanocrystalline Co_3O_4, its performances in CO oxidation, lithium-ion battery, and some other emerging fields and facet-dependent behaviour. Scheme 1 shows the design, synthesis, structure and applications relating to the Co_3O_4 nanocrystals with predominantly exposed crystal planes. The design is generally orientated by the practical applications, which require better performances of the material. Synthesis protocols will be then investigated to obtain the material with desired properties by structural control. The mechanism of the enhanced performances of the material can be described by the crystal structure and microstructure, both of which promote the applications of the material and sometimes, bring out break-through science and emerging applications.

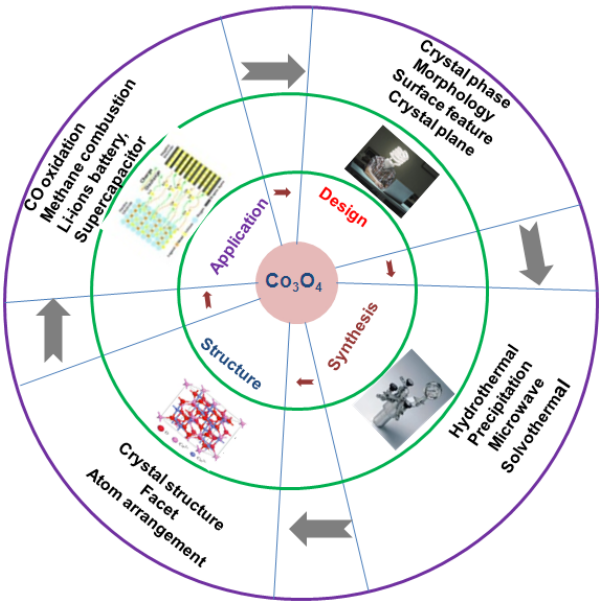

Scheme 1 Research activities and their correlation to Co_3O_4 with predominantly exposed facets

2. Synthesis of Co_3O_4 with selected facets

The preferentially exposed crystal planes of Co_3O_4 can be achieved by manipulation of the morphology, which is feasible as shape-controlled synthesis. Fig. 1 shows SEM and TEM images of some typical Co_3O_4 nanostructures such as nanowires, nanospheres, nanorods, nanosheets, nanobelts and nanocubes. The close relationship between geometric shape and crystal plane determines a rational design of the crystal facets in a controlled synthesis.

Generally, the synthesis can be achieved by hydrothermal and solvothermal methods. The crystal shapes can be controlled by addition of surfactant, solution temperature, and ratio of precursors. In which, a surfactant such as cetyl trimethylammonium bromide (CTAB) can be the most important preparation parameter as a morphology-directing agent, template, or capping agent in the formation of the desired low dimensional nanostructures.[55] Solution temperature would significantly control the speed of crystal growth and the redissolving and redepositing process, and the precursors can control both the chemical compositions and morphologies of the nanocrystals.[56]

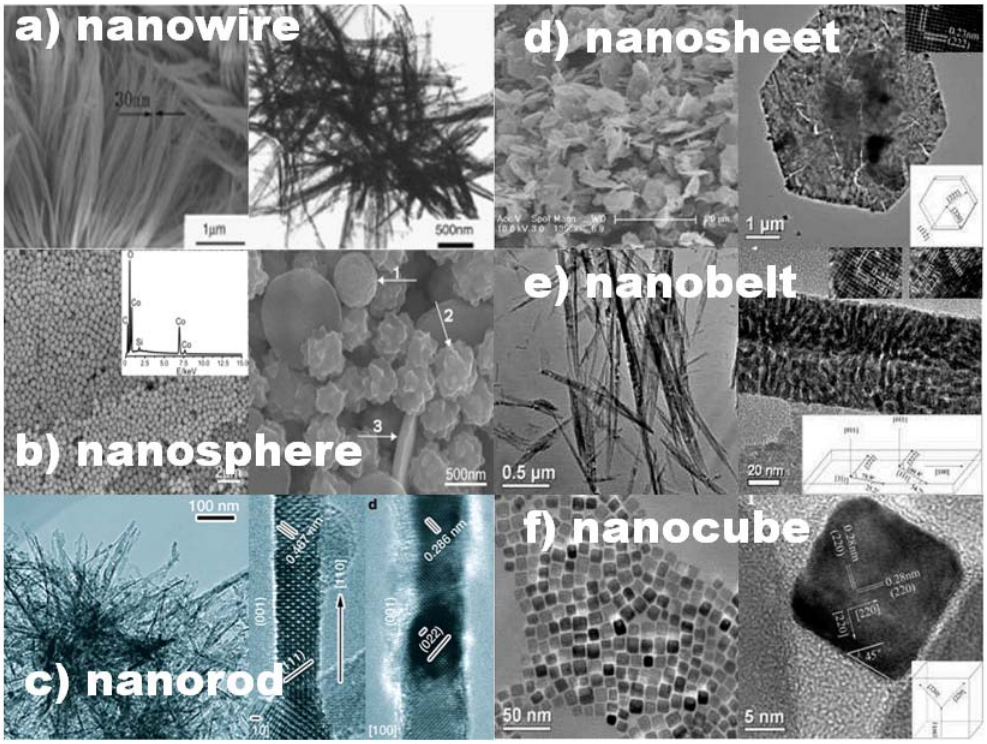

Figure 1 Nanocrystalline Co_3O_4 with various morphologies, a) nanowires, reproduced from Ref. [27] with permission from Elsevier, b) nanosphere, reproduced from Ref. [14] with permission from ACS, c) nanorods, reproduced from Ref. [7] with permission from Nature Publishing, d) nanosheet, e) nanobelt, and f) nanocube, d)-f) reproduced from Ref. [24] with permission from ACS.

2.1. Hydrothermal synthesis

Hydrothermal methods have been widely used for preparation of nanomaterials. The autogenerated pressure from water upon heating can further enhance the solubility and the

reactivity of the reactants to improve the crystallinity of the prepared nanocrystals. Moreover, small coordinating molecules (e.g. NH_3, ethylenediaminetetraacetic acid) can be easily introduced to adjust the growth of the final nanocrystals. The strong polarity of water might be beneficial to the orientation growth of 1 D nanostructures.[53]

Li et al. [24] reported a rational synthesis of Co_3O_4 with different shapes via a hydrothermal process of cobalt hydroxide precursors. It was found that the predominantly exposed planes are {112} in the nanosheets, {011} in the nanobelts, and {001} in the nanocubes. The key parameter in the shape-controlled synthesis was the precursor of β-$Co(OH)_2$ nanosheets and $Co(CO_3)_{0.5}(OH)0.11H_2O$ nanobelts.

Crystalline Co_3O_4 nanospheres with non-orientation, nanocubes with {100} orientation, and rhombododecahedrons with {110} orientation, were obtained hydrothermally using differently charged surfactants and solvents.[57] *N*,*N*-dimethylformamide (DMF) and acetonitrile were employed for preparation of rhombododecahedrons, hexadecyltrimethyl-ammonium chloride (CTAC) or sodium dodecyl sulfate (SDS) for nanocubes, and Triton X-100 for nanospheres. Scheme 2 displays the possible mechanism for Co_3O_4 polyhedron formation using different surfactants. Charge density, atom density and dipolar moment were major factors influencing the specific interactions between changed capping agents and crystal planes of Co_3O_4 to the selective formation of cubes with {100} orientation, and rhombododecahedrons with {110} orientation. The neutral chains of non-ionic surfactant cause the non-selective adsorption on the crystal surfaces, leading to the formation of spheres without specific orientation. In the presence of ionic surfactants, CTAC and SDS, the charged R_4N^+ and SO_4^{2-} groups of the surfactants preferentially adsorbed on highly charged {100} planes rather than relatively less charged {110} planes, resulting in the growth inhibition of {100} planes and formation of nanocubes. The polar DMF and acetonitrile as weak capping agents cannot compensate the system energy increase and will then be adsorbed on the stable {110} planes, producing the rhombododecahedrons.

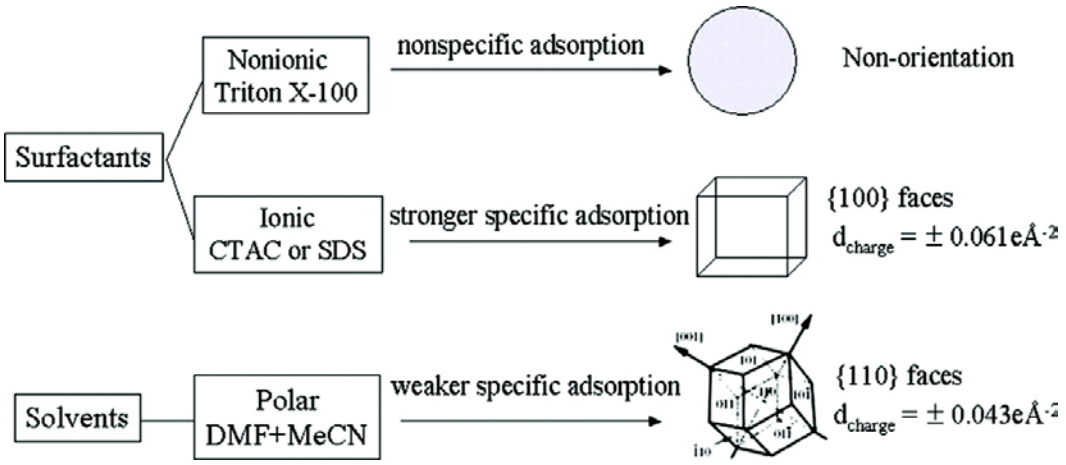

Scheme 2 Possible mechanism for Co_3O_4 polyhedrons synthesized in the presence of different charged surfactants and solvents. Reproduced from Ref. [57] with permission from ACS.

A 2-D functionalized Co_3O_4 nanomesh with the dominant $\{\bar{1}12\}$ crystal planes was prepared by the formation of single crystal $(NH_4)_2Co_8(CO_3)_6(OH)_6 \cdot 4H_2O$ nanosheet as the precursor and its subsequent conversion upon calcination. [35] Ethylene glycol, concentrated $NH_3 \cdot H_2O$, Na_2CO_3 and $Co(NO_3)_2$ were used to prepare the nanosheet precursor via a hydrothermal process at 160 – 200 ^oC for 12 – 48 h. The produced nanomesh had a higher surface area as compared to the other Co_3O_4 nanostructures, well-crystallized features, thickness of no more than 10 nm and a void space diameter below 6.0 nm. Fig. 2 shows the HRTEM images and the difference in the exposed crystal planes of selected samples. The dominant $\{\bar{1}12\}$ crystal plane in the nanomesh was of much better performance for electrochemical energy storage than the conventional {111} and {100} planes. Besides the benefits from unique morphology and structure, the better performance of $\{\bar{1}12\}$ plane than conventional planes was attributed to the higher surface energy.

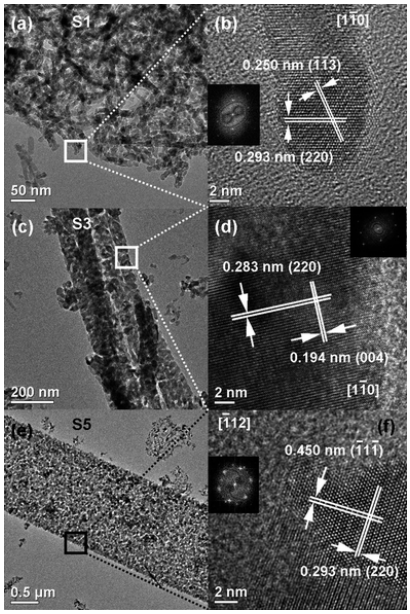

Figure 2 The difference in the exposed crystal planes of the final products of S1, S3 and S5. S1 has a diameter of 15 nm (a) with the addition of 1 mL Na_2CO_3 aqueous solution (1 M); S3, 150 nm, 1.5 mL Na_2CO_3 aqueous solution; S3, 1000 nm, 10 mL Na_2CO_3 aqueous solution. S1 and S3, whose precursor is $Co(CO_3)_{0.5}(OH)0.11H_2O$, exhibit the exposed crystal plane of $(1\bar{1}0)$ on the largest scale (a–d), whereas S5 with $(NH_4)_2Co_8(CO_3)_6(OH)_6{\cdot}4H_2O$ as precursor, exposes the crystal plane of $(\bar{1}12)$ on the largest scale (e and f). Reproduced from Ref. [35] with permission from RSC.

Nanocrystalline Co_3O_4 samples with plate-like shape of {111} predominant plane, rod-like shape of {110} predominant plane, cubical of {100} predominant plane, and roughly spherical morphologies of multiple planes were fabricated using $CoCl_2$ with or without capping reagent via hydrothermal processes. [58] The plate-like Co_3O_4 prepared by $CoCl_2$, poly(vinylpyrrolidone) (PVP, Mw = 35 000) and KOH mainly exposed {111} crystal plane, and showed the highest activity in catalytic CO oxidation.

Three types of Co_3O_4 with different well-defined crystal plane structures, including a cube with {001} plane, a truncated octahedron with {001} and {111} planes, and an octahedron with the {111} plane were successfully prepared by a one-step hydrothermal method. [59] The shape control was facilely achieved by simply adjusting the ratio of NaOH and cobalt precursor of $Co(NO_3)_2{\bullet}6H_2O$, without any capping reagent. When the starting concentrations of $Co(NO_3)_2{\bullet}6H_2O$ and NaOH were 0.04 and 0.01 mol/L, Co_3O_4 cubes were obtained. On the other hand, when the concentrations were 0.08 and 0.01 mol/L, truncated octahedron was prepared, and if at 0.20 and 0.05 mol/L octahedron was obtained.

Zhu et al. [60] reported that rhombus-shaped Co_3O_4 nanorod arrays grown directly on a nickel substrate were successfully synthesized by a fluorine-mediated hydrothermal approach. The prepared nanorods were quasi-single-crystalline in nature with an axis perpendicular to the {202} plane, showing growth along the [101] direction. It was suggested that the nanorods were enclosed by two equivalent $\{12\bar{1}\}$ crystal planes and two equivalent $\{10\bar{1}\}$ crystal planes. The formation of Co(OH)F in the synthesis was found to play the crucial role in producing the nanorod arrays.

2.2. Precipitation synthesis

Precipitation method is very simple, but the precise control of the orientation usually needs the assistance of surfactant or coordinating molecules. Nanorod-shaped Co_3O_4 nanocrystals with exposed {110} planes were prepared by the calcination of a cobalt hydroxide carbonate precursor, which was synthesized by the precipitation of cobalt acetate with sodium carbonate in ethylene glycol.[7] In the design, a solid cobalt hydroxide carbonate, incorporating ethylene glycol and having a nanorod-shape structure with a diameter of 10 - 20 nm and a length of 200 - 300 nm, was prepared and then used as the precursor for further calcination. Sharma et al. reported a formation process of Co_3O_4 nanorods by a controlling assembly of oxide nanoparticles, shown in Scheme 3.[61] The formation process followed an oriented aggregation of Co_3O_4 nanoparticles of varying shapes and sizes. The cationic surfactant of CTAB played an important role in the formation of rod-like morphology by decreasing the surface charge density of ionic micelles and thereby promoting the formation of micellar geometries like nanorods.

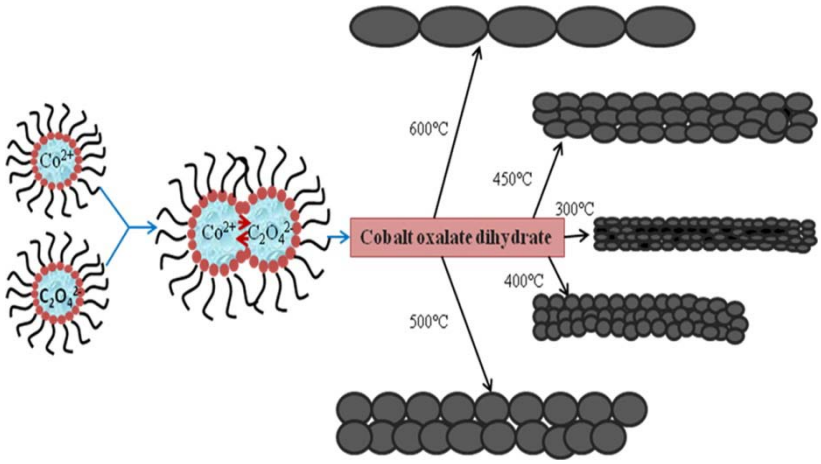

Scheme 3. Schematic formation process of Co_3O_4 nanorods. Reproduced from Ref. [61] with permission from RSC.

Lin et al.[62] reported a simple method to prepare highly dispersed Co_3O_4 nanocubes by aqueous precipitation method at low temperature (70 – 90 ^oC). It was found that ammonia as the precipitator was essential to achieve cubic-like Co_3O_4 nanoparticles. The precipitator might play the role in determining the orientation growth of the nanocrystals, and would strongly influence the morphology of the objective materials.

2.3. Other synthesis and short summary

Ultrathin Co_3O_4 nanowires with exposed {111} planes was fabricated by oriented attachment. [39] The heating temperature controls the diameter of nanowires and the thickness of nanowalls. Meanwhile, the heating duration determines the size of nanowires (< 300 ^oC) and nanowalls (> 300 ^oC). The thinnest Co_3O_4 nanowires grew by oriented attachment of atomic Co_3O_4 building blocks one by one along the [110] direction. The smallest building block along the wire has four Co^{3+} cations, two Co^{2+} cations, and eight O^{2-} anions. To keep the Co/O ratio as 3/4, the Co^{3+} in the middle of the smallest building blocks were removed during the formation of the wires. Therefore, the distance of about 0.57 nm between the Co^{3+} cations along the axis of the thinnest wire is the twice that in bulk Co_3O_4 in the [110] direction. Then the smallest building blocks of Co_3O_4 could adopt correct positions along the [110] direction to develop the long-range-ordered crystalline lattice of nanowire.[63] At a higher temperature, the accumulation of the Co_3O_4 is much quick to form thicker edges and the sharp corners at the surface were passivated to produce nanowalls. The nanowalls constructed by the smallest building blocks are preferentially exposing the {111} planes, which mainly composed of Co^{3+} cations.[39, 63] The study indicated that the Co_3O_4 nanowires and nanowalls were grown by one-dimensional (1-D) and two-dimensional (2-D) oriented attachment of atomic Co_3O_4 building blocks, respectively.

It was reported that self-stacked Co_3O_4 nanosheets with mainly exposed of {111} planes were prepared by a solvothermal method in the presence of poly(vinylpyrrolidone) (PVP) and water followed by a calcination treatment.[64] Both PVP and water would significantly affect the formation of self-stacked nanosheet ensembles. The presence of water can partially decrease the coverage of PVP on the produced nanoplate surface, then results in the

preferential adsorption of PVP on the top and bottom surfaces of the nanoplates, within which the growth of nanocrystals occurs.

Table 1 lists a variety of nanocrystalline Co_3O_4 particles with their synthesis methods and predominantly exposed planes. The table shows that there are available approaches to obtain selected facets by shape-controlled synthesis.

Table 1 Shape, preparation, and facet of various Co_3O_4 nanocrystals

Morphology	Precursor	Synthesis	facet	Ref.
Sphere	$Co(NO_3)_2$•$6H_2O$, methanol, sodium dodecylbenzenesulfonate (SDBS)	Surfactant-assisted solvothermal decomposition	N/A	65
Sphere	$Co(CH_3COO)_2$•$4H_2O$, (poly(vinylpyrrolidone) PVP, ethylene glycol	Polyol process	N/A	14, 66
Sphere	$Co(NO_3)_2$•$6H_2O$, ethylene glycol	Hydrothermal	{111}	67
Cube	$Co(CH_3COO)_2$•$4H_2O$, ammonia solution, ethanol	Hydrothermal	N/A	6, 68
Cube	$Co(CH_3COO)_2$•$4H_2O$, ammonia solution, sodium oleate (SOA), hydrogen peroxide	Aqueous precipitation	N/A	62
Cube	$Co(NO_3)_2$•$6H_2O$, hydrogen peroxide, water, ammonia solution	Hydrothermal	{100}	69
Sheet	$Co(NO_3)_2$•$6H_2O$, hydrogen peroxide, hexamethylenetetramine (HMT)	Precipitation	{111}	70
Sheet	$Co(NO_3)_2$•$6H_2O$, methanol, water	Alcoholysis	{111}	71
Sheet	$Co(CH_3COO)_2$•$4H_2O$, (poly(vinylpyrrolidone) PVP, ethylene glycol	Solvothermal	{111}	64
Belt	$CoCl_2$•$6H_2O$, hexadecyltrimethyl-ammonium chloride (CTAC), *N*,*N*-dimethylformamide (DMF), hydrogen peroxide	Hydrothermal	$\{11\bar{2}\}$	30
Belt	$Co(NO_3)_2$•$6H_2O$, glycerol alcohol, water	Hydrothermal	{011}	24, 72
Belt	$Co(CH_3COO)_2$•$4H_2O$, $Co(OH)_2$, 1,2-propanediol, ammonia	Hydrothermal	{111}	73
Rod	$CoCl_2$•$6H_2O$, 1,10-phenanthroline, water, NaCl, KCl	Precipitation	{-1,-1,15}	74
Rod	$Co(NO_3)_2$•$6H_2O$, ammonium fluoride, hexamethylenetetramine (HMT), water	Fluorine-mediated hydrothermal	$\{12\bar{1}\}$, $\{10\bar{1}\}$	60
Rod	$Co(CH_3COO)_2$•$4H_2O$, ethylene glycol, Na_2CO_3	Precipitate	{110}	7
Plate	$CoCl_2$•$6H_2O$, KOH	Microwave hydrothermal	{111}	75

Tube	$Co(NO_3)_2$•$6H_2O$, ammonia solution, water	Precipitation	{111}	[76]
Tube	CoC_2O_4•$2H_2O$, NaOH	Interfacial reaction	{112}	[77]
Wire	Cobalt fossil, water, air	Heating cobalt fossil	{111}	[39, 78]
Wire	$Co(NO_3)_2$•$6H_2O$, NH_4F, water, $CO(NH_2)_2$,	Hydrothermal	{110}	[79]
Octahedron	$CoCl_2$•$6H_2O$, thiourea, ethylene glycol	Microwave synthesis	{111}	[80]
Mesh	$Co(NO_3)_2$•$6H_2O$, ammonium hydroxide, sodium carbonate	Hydrothermal	$\{\bar{1}12\}$	[35]

3. Co_3O_4 preferential-facet promoted applications

3.1. Catalysis in environmental and energy application

3.1.1. Low temperature CO oxidation

The catalytic oxidation of CO has been intensively studied,[81] owing to its significance in environmental[82] and fundamental applications.[72] Gold catalysts,[83-85] ruthenium catalysts,[86, 87] and Co_3O_4-based catalysts [39, 82, 88-91] have been demonstrated effective for low temperature CO oxidation. In which Co_3O_4 has been extensively investigated due to its high catalytic activity and low cost compared to noble metals. However, the low temperature activity of Co_3O_4 would be inhibited by the presence of water, hydrocarbons and NO.[7, 82, 89] Morphological chemistry of Co_3O_4 was applied to prepare its nanocrystallites with different shapes, by which the effects of preferential facets on the performance at low temperature CO oxidation were investigated.

Nanorod-shaped Co_3O_4 with predominantly exposed {110} planes was showing not only surprisingly high catalytic activity in CO oxidation at temperature as low as -77 ^oC but sufficient stability in feed gases containing large amounts of H_2O and CO_2 at 200-400 ^oC.[7] Fig. 3 shows the nature of the enhanced performance of Co_3O_4 nanorods in CO oxidation. Fig. 3(a) shows that in the spinel Co_3O_4, the Co^{3+} in an octahedral coordination was found to be the active site for CO oxidation, while Co^{2+} in a tetrahedral is inactive. Fig. 3(b-d) shows {001} and {111} planes only have Co^{2+} cations, but {110} planes is mainly made of Co^{3+} cations. Fig. 3(e) therefore shows the reaction pathways, indicating CO molecules interact preferably with the surface Co^{3+} cations, which were enriched by rod-shape with preferable {110} facets.

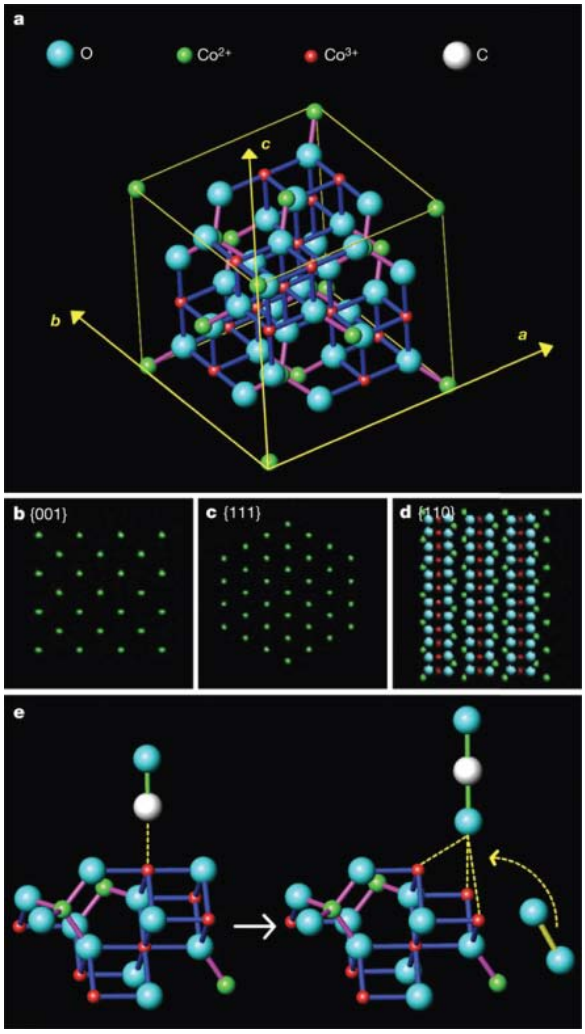

Figure 3 a, Spinel structure of Co_3O_4 crystal. **b**–**d**, The surface atomic configurations in the {001} (**b**), {111} (**c**), and {110} (**d**) planes. **e**, A ball-and-stick model for CO adsorption and oxidation on the active Co^{3+} site. Reproduced from Ref. [7] with permission from Nature Publishing.

In another report, CO oxidation was performed on Co_3O_4 nanobelts and nanocubes.[72] It was found that the Co_3O_4 nanobelts with exposed {011} planes were more active than nanocubes with {001} planes. Fig. 4 shows the catalytic properties of differently shaped Co_3O_4 nanocrystals. The specific rate of conversion over nanobelts at 56 ^oC is 1.37 times higher than that over nanocubes. The turnover frequency (TOF) of Co^{3+} sites of {011} planes on Co_3O_4 nanobelts was far higher than that of {001} planes on nanocubes. At 56 ^oC, the turn-over-freqency (TOF) of Co^{3+} sites on the naobelts is 7.4×10^{-3} s^{-1}, while only 2.7×10^{-3} s^{-1} for the nanocubes, indicating that TOF of Co^{3+} sites on {011} plane is 2.7 times higher than {001}

planes. The difference in catalytic activity was attributed to the different locations of Co^{3+} sites.

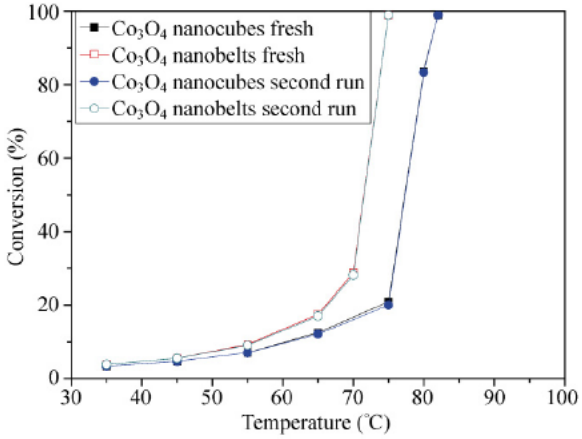

Figure 4 CO conversion as a function of reaction temperature over Co_3O_4 nanobelts and nanocubes. Reproduced from Ref. [72] with permission from Springer.

Fig. 5 (a) and (b) show the active Co^{3+} sites on the surface layer of the {011} planes of nanobelts. Fig. 5(c) and (d) reveal those on the first sub-layer of {001} planes of nanocubes. The adsorption of CO on the first sub-layer of Co^{3+} sites would be more difficult than on the topmost surface layer of Co^{3+} sites, leading to the fact that {011} planes of nanobelts are more active than {001} planes of nanocubes.[72]

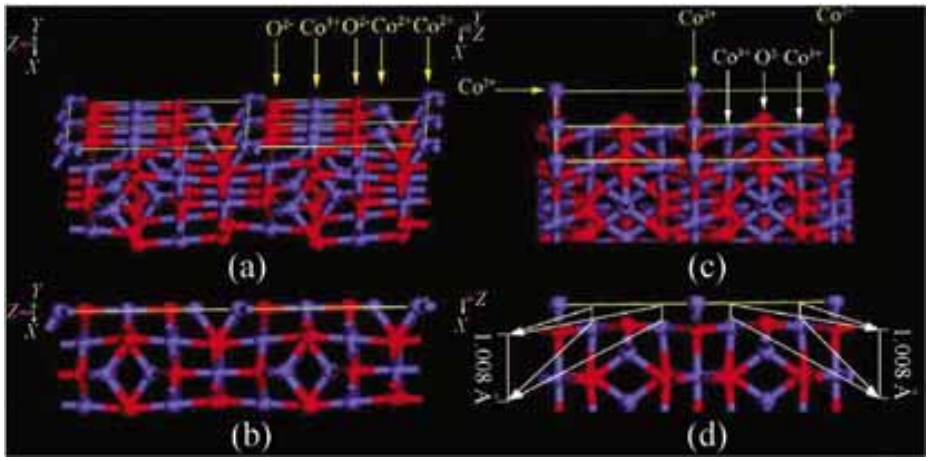

Figure 5 (a) Surface atoms of the Co_3O_4 {011} plane. (b) Horizontal view of the Co_3O_4 {011} plane. (c) Surface atoms of the Co_3O_4 {001} plane, (d) Horizontal view of the Co_3O_4 {001} plane. Atoms highlighted with yellow arrows are located on the surface layer of the plane,

and those with white arrows on the first sub-layer of plane. Reproduced from Ref. [72] with permission from Springer.

Teng et al. [58] investigated the catalytic activities of Co_3O_4 nanocrystals with different shapes (plates, rods, cubes and spheres) in CO oxidation. Fig. 6 shows light-off curves of CO oxidation obtained from the four samples. CO oxidation occurred at temperature below 273 K, and the T_{50} (reaction temperature at 50% conversion) values for nanoplates, nanorods, nanocubes and nanospheres of Co_3O_4 were 190, 218, 225, and 230 K, respectively. The results indicated that plate-like Co_3O_4 with predominantly exposed {111} planes showed the highest catalytic activity for CO oxidation. In the study, the activities were evaluated under dry stream, which is close to ideal condition assumed in computational calculation. By which, it was found that {111} planes expose a stable outmost surface after relaxation, meanwhile surface relaxation of the {110} planes is not significant.[92, 93]

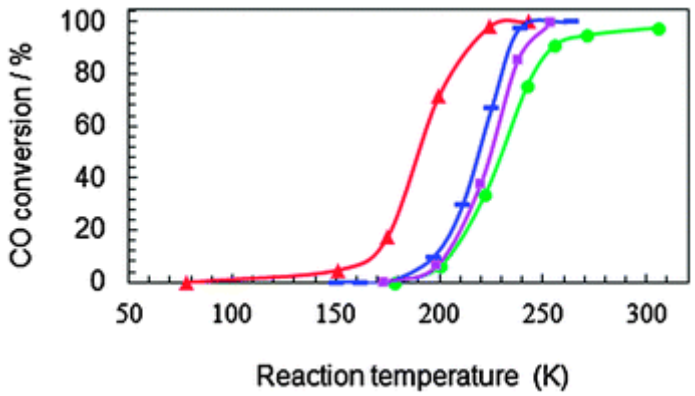

Figure 6 Conversion as a function of temperature for CO oxidation over differently shaped Co_3O_4 nanocrystals: (▲) plate, (–) rod, (■) cube, and (●) sphere. Reproduced from Ref. [58] with permission from RSC.

He et al. [39] also discovered that ultrathin Co_3O_4 nanowires with exposed {111} planes have a high activity for CO oxidation. The high activity was ascribed to the larger surface area and the abundance of active Co^{3+} on the surface.

Theoretical studies were carried out to find out the origin of extraordinary catalytic activity of Co_3O_4 and the related morphological chemistry in low temperature CO oxidation. The elementary reactions of CO oxidation on the commonly exposed surfaces of Co_3O_4, {110}-A,

{110}-B, {111} and {100} were investigated. It was found that Co^{3+} is the active site rather than Co^{2+}. Moreover, the three-coordinated O bonded with three Co^{3+} may be slightly more reactive than the other two kinds of lattice oxygen, that is, the two-coordinated O bonded with one Co^{2+} and one Co^{3+} and the three-coordinated O bonded with one Co^{2+} and two Co^{3+}. The study further showed that CO adsorption strength, the barrier of CO reacting with lattice O and the redox capacity would be identical to be the determining factors that would significantly affect the activity of oxides.[91]

3.1.2 Methane combustion

Selected shape or facet of Co_3O_4 was also found to have promotive performances in methane combustion. Li et al. [24] investigated the effects of shape and crystal planes, including nanosheets with predominantly exposed {112} planes, nanobelts with {011} and nanocubes with {001} on the catalytic behaviour of methane combustion. Fig. 7 shows the catalytic properties of different shape Co_3O_4 nanocrystals. The CH_4 conversion was 50% over Co_3O_4 {112}, 42% over Co_3O_4 {011}, and 23% over {001} planes of Co_3O_4 at 313 °C, with the specific rates of 2.72, 2.28, and 1.25 μmol g^{-1} s^{-1}, respectively. The specific rate of CH_4 conversion over Co_3O_4 nanosheets at 313 °C was found to be two times higher than that over nanocubes and 19% higher than that over nanobelts. The activities showed that the Co_3O_4 nanosheets were more active than Co_3O_4 nanobelts and nanocubes. It was found that catalytic activity order for methane combustion on the crystal planes were {112} > {011} >> {001}. The surface atom arrangement of the Co_3O_4 with different planes was suggested to be responsible for the different catalytic activities.

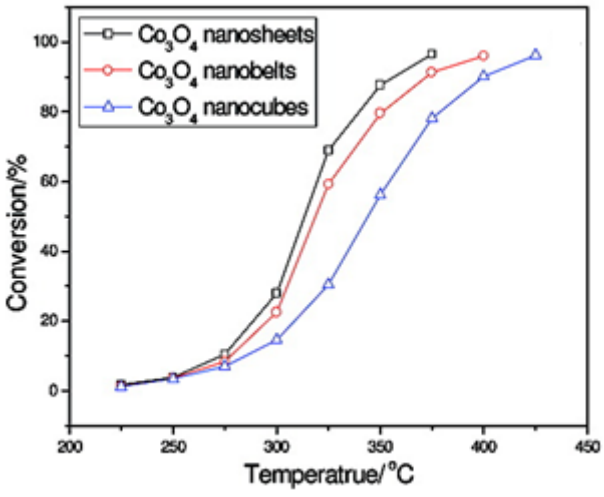

Figure 7 Methane conversion as a function of temperature over Co_3O_4 nanosheets, nanobelts, and nanocubes. Reproduced from Ref. [24] with permission from ACS.

Hao et al.[94] studied the catalytic activity of octahedra with predominantly exposed {111} facets of Co_3O_4 in methane combustion. The Co_3O_4 octahedra had no catalytic activity, while the irregular shaped Co_3O_4 nanoparticles prepared by a conventional precipitation method were highly active at the same reaction conditions, indicating Co_3O_4 with low surface energy results in low catalytic activity in methane combustion. Above two studies suggested that the catalytic activity can be feasibly controlled by preparation of shape-controlled Co_3O_4 with selected facets.

3.1.3. Ethylene oxidation

Mesoporous Co_3O_4 with selected facets also showed very high activity for low temperature oxidation of trace ethylene. It was found that {110} facets were the exposed active surfaces of mesoporous Co_3O_4 replicated from 3-D cubic KIT-6 silicas, while the Co_3O_4 nanosheets had predominantly exposed {112} facets.[95] In the oxidation of trace ethylene, mesoporous Co_3O_4 with {110} planes was more active than Co_3O_4 nanosheets with {112} planes. Table 2 compares the ethylene oxidation activities and physical properties of various catalysts. It was found that Co_3O_4 with {110} planes showed a high ethylene oxidation at 0 ^oC, while no activity was observed over Co_3O_4 nanosheets with {112} planes. The {110} planes are composed mainly of Co^{3+} cations, which were regarded as the active sites for ethylene oxidation, and then the abundant Co^{3+} cations on the {110} planes would provide sufficient sites for ethylene. It was concluded that the {110} planes are the mainly active planes for ethylene oxidation.[95] In the further study, three different shaped Co_3O_4 (nanorods, nanopolyhedra and nanocubes) were used to prepare supported Au catalysts. Compared with {011} and {001} planes, {110} planes showed the maximum amount of oxygen vacancies, which play a major role in ethylene oxidation.[96]

Table 2. Ethylene oxidation activities and physical properties of Co_3O_4 and Au/Co_3O_4 catalysts. Reproduced from Ref. [95] with permission from ACS.

Catalysts	**C_2H_4 conversion (%)**	**S_{BET} (m^2/g)**	**V_p(cm^3/g)**	**D_p (nm)**
Co_3O_4 ({110} facets)	30 (0 °C)	84	0.14	3.6/11.7

Catalysts	C_2H_4 conversion (%)	S_{BET} (m^2/g)	V_p(cm^3/g)	D_p (nm)
1.0% Au/Co_3O_4 ({110} facets)	50 (0 °C)	94	0.17	3.4/11.4
2.5% Au/Co_3O_4 ({110} facets)	76 (0 °C)	100	0.18	3.4/11.5
Co_3O_4 ({112} facets)	0 (20 °C)	–	–	–
2% Au/Co_3O_4 ({112} facets)	7.4 (20 °C)	–	–	–

3.1.4. Hydrodesulfurization (HDS)

The hydrogenation of carbonyl sulphide (COS) was carried out over catalysts derived from nanocrystalline Co_3O_4 nanorods and nanopolydedra. Nanorods showed a high activity in presulfurization process and resultant sulfide was superior to nanopolyhedra in HDS of carbonyl sulphide. It was known that nanrods are enclosed by four {110} and two {001} planes, and nanopolyhedra are enclosed by eight {111} and six {100} planes. The exposure of {110} surface might lead to the stronger reactive property of nanorods than nanopolyhedra, and facilitated the formation of more sulphur species on the rods during presulfurization stage, then increase hydrodesulfurization activity for COS.[97]

3.2. Electrochemical performance in energy storage

3.2.1. Lithium-ion battery

Rechargeable lithium-ion batteries are key components of a large range of modern portable equipments for entertainment, computing and telecommunication. As an energy storage unit, Li-ion battery offers high energy density, flexible and lightweight design and longer lifespan than comparable battery technologies. [98] A battery is a device that converts chemical potential to electric energy through Faradic reactions and consists of three basic components: an anode, a cathode, and an electrolyte. Electrode materials must fulfil three fundamental requirements: (i) a high specific charge and charge density, (ii) a high cell voltage, resulting from a high (cathode) and low (anode) standard redox potential of the respective electrode redox reaction, and (iii) a high reversibility of electrochemical reactions at both cathodes and anodes.[99, 100] In the most popular Li-ion battery, a graphite anode (mesocarbon, microbeads, or MCMB (MesoCarbon MicroBeads)), a cathode made by lithium metal oxide ($LiMO_2$, e.g. $LiCoO_2$) and an electrolyte having a solution of lithium salt (e.g. $LiPF_6$) in a mixed organic solvent (e.g. ethylene carbonate-dimethyl carbonate, EC-DMC) imbedded in a separator felt. In 2000, it was reported that electrodes made of nanoparticles of transition-metal oxides (MO, where

M is Co, Ni, Cu or Fe, and Co_3O_4 in particular) demonstrated electrochemical capacities of 700 mA h g^{-1}, two to three times larger than those that use graphite as the anode electrode, with 100% capacity retention for up to 100 cycles and high recharging rates.[101] However, they usually suffer from poor capacity retention upon cycling and /or poor rate capability. Traditional electrode materials have large volume changes during repeated lithium uptake and removal reactions, and then produce local stress and eventually lead to electrode failure. A promising strategy to resolve the problems was to prepare nanosized materials with designed structures and morphologies. Nanosized materials can offer unusual mechanical, electrical, and optical properties from their low dimensions in geometry, and behave the integrated functions of bulk and surface properties. In lithium-ion battery, nanostructures would provide huge surface area, short mass and charge diffusion distance, and freedom for volume change during charge-discharge cycles, and eventually improve the Li-ion intercalation properties. [76, 102]

Li et al. [103] investigated the lithium storage properties of complex structures, such as cobalt oxide-coated cobalt hydroxide carbonate nanowires, cobalt oxide nanotubes and porous cobalt oxide nanowires. At a high charge/discharge current density of 100 mA g^{-1}, the nanotubes, nanowires, and hollow spheres were capable of retaining a specific capacity of 893, 847, and 686 mAh g^{-1} with average fading rates of 0.54, 0.32 and 0.61% per cycle over 40 cycles, respectively. The improved electrochemical properties were ascribed to smaller size, porous structure, and favourability for electron transportation and insertion and extraction of lithium ions of 1-D nanostructures of Co_3O_4. [103]

Both theoretical [104] and experimental [105, 106] studies indicated that the crystal plane structure would significantly influence the Li^+ transport and the electrochemical performance. A comprehensive study was conducted to investigate the effect of crystal plane on the electrochemical performance of Co_3O_4. [59] Three nanocrystalline Co_3O_4 with different shapes and preferential facets, including a cube with the {001} plane, a truncated octahedron with {001} and {111} planes, and an octahedron with the (111) plane, are prepared and shown in Fig. 8.

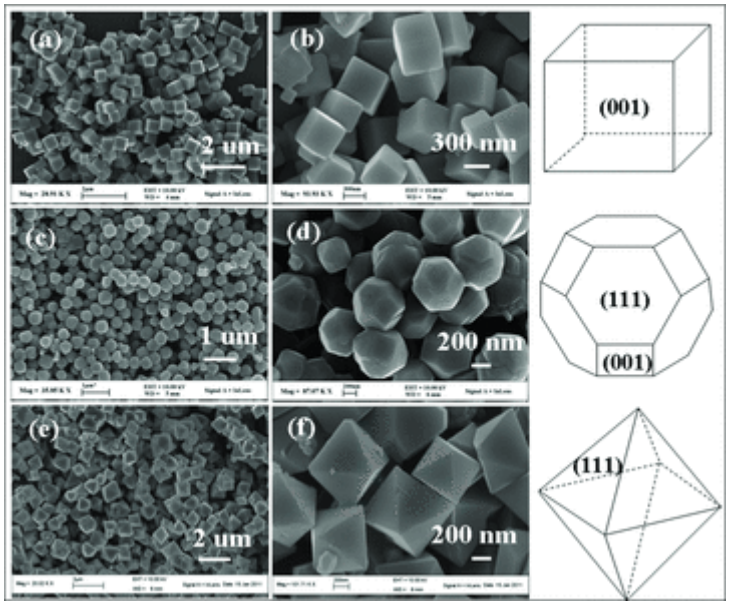

Figure 8 SEM images of the three types of calcined Co_3O_4 and their structure models: a,b) Co_3O_4 cubes, c,d) Co_3O_4 truncated octahedra, and e,f) Co_3O_4 octahedra. Reproduced from Ref. [59] with permission from Wiley-VCH.

Fig. 9 displays the charge/discharge curves of the differently shaped Co_3O_4 nanocrystals. The results showed that the first discharge and charge capacities were 969 and 795 mAh g^{-1} for Co_3O_4 cubes, 1023 and 990 mAh g^{-1} for Co_3O_4 truncated octahedra, and 1098 and 991 mAh g^{-1} for Co_3O_4 octahedra. All the first discharge capacities were higher than the theoretical capacity of Co_3O_4, which might be attributed to the formation of a solid electrolyte interphase (SEI) layer and possibly interfacial lithium storage. The Co_3O_4 octahedron with the {111} plane has the highest reversible capacity and the best rate capacity. It was further discovered that the electrochemical performance of Co_3O_4 can be ranked as octahedron > truncated octahedron > cube, and the {111} plane may be more beneficial to Li^+ transport than the {001} plane.[59] The high voltage plateau of Co_3O_4 nanocrystals was about 1.2 V, compared to 0.2 V of carbon/graphite anode, making them possible to overcome the shortcomings of graphite as anode materials. For a good battery voltage, high voltage cathode materials, such as $LiMn_{1.5}Ni_{0.5}O_4$ or $LiNi_{0.5-x}Al_{2x}Mn_{1.5-x}O_4$ at 5 V, can be used.[107, 108]

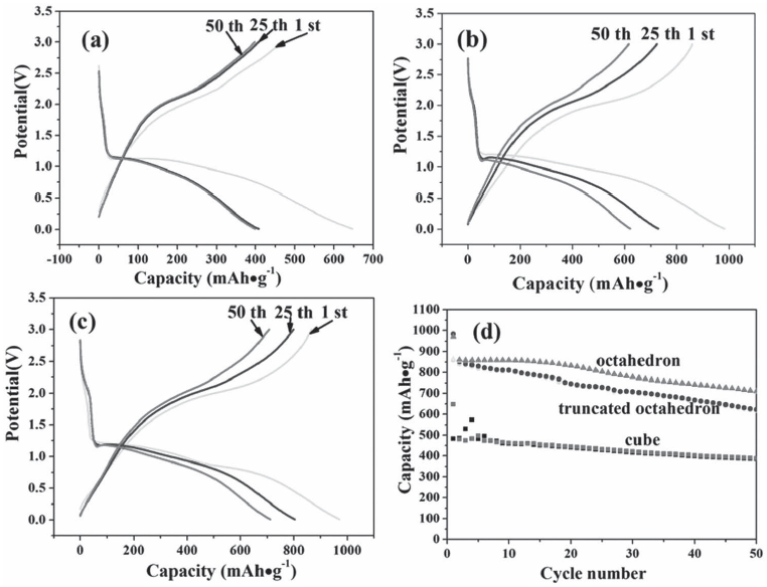

Figure 9 The charge/discharge curves of a) Co_3O_4 cubes, b) Co_3O_4 truncated octahedra, and c) Co_3O_4 octahedra for the 1st, 25th, and 50th cycles between 0.01 and 3.0 V at a rate of 1000 mA g^{-1}. d) Comparison of cycling performance of the three kinds of Co_3O_4. Reproduced from Ref. [59] with permission from Wiley-VCH.

Huang et al.[109] prepared porous Co_3O_4 with the hexagonal sheet-like morphology (H-Co_3O_4) of main (111) planes. The H-Co_3O_4 electrode showed excellent cycleability and rate capacity, and the superior electrochemical performance was attributed to the porous 2D structures with a finite lateral size and enhanced open-edges. Moreover, the exposed (111) planes are very active and can improve the capacity retention and rate performance. Based on the studies on Co_3O_4 nano-octahedra enclosed by {111}, Sun et al.[36] suggested that the relationship between the {111} facets and the good electrochemical performance could be attributed to the surface atomic arrangement of the facet. The (111) plane has a more open surface structure than (100) and (110) planes, which could offer more active sites for the diffusion of lithium ions. Moreover, there are fewer interlayer spacing and tunnels through the direction of [100] and [110], so the diffusion of Li ions through them would be more difficult than that through [111].

3.2.2. Supercapacitors

Electrochemical capacitors are promising sources for many portable systems and automotive applications. A number of transition metal oxides have been suggested as alternative

electrodes such as Co_3O_4, MnO_2, and NiO etc., to hydrated ruthenium oxide due to its high cost. However, such electrode materials lead to low capacitance, poor rate capability, and deterioration in performance associated with faradic redox reaction.[110] It was suggested that electrodes with designed nanostructures would be possible to enhance not only power density but also cycling stability. [111, 112]

Qian et al. [23] reported that the specific capacitance of Co_3O_4 nanosheets was higher than that of the Co_3O_4 microsphere in a KOH electrolyte solution. The Co_3O_4 nanosheet electrodes also exhibited good rate capabilities, and maintained 93% of initial capacity at a current density of 5 mA cm^{-2} in a KOH electrolyte solution. The improved electrochemical performance was attributed to the mesoporous structure, which might provide a large surface area that favours good contact with electrolytes.

Three Co_3O_4 samples with distinct morphologies, 1-D needle like nanorods, 2-D leaf-like nanosheets, and 3-D oval-shaped microparticles, were tested for their potential application as supercapacitors.[9] The results indicated that these porous Co_3O_4 structures exhibited promising capacitive properties with high capacitance and good retention. Co_3O_4 nanorods also showed the highest capacitance of 111 F g^{-1}, and 88.2% of which can still be maintained after 1000 charge-discharge cycles. However, the rate capability and capacitance retention were still unsatisfactory. In order to improve the electrochemical performance of electrode materials for supercapacitors, the issues, such as double layer capacitance, faradaic capacitance from surface redox process and faradaic contribution from the diffusion-dominated interaction between electrolyte ions and electrode materials, should be considered.[113]

Wang et al. [35] discovered a novel 2-D functional Co_3O_4 nanomesh, which had a very high surface area (382 m^2 g^{-1}), well-crystallized features, thickness of no more than 10 nm and a void space diameter below 6 nm. They reported that the dominant $\{\bar{1}12\}$ crystal plane in the nanomesh has much higher surface energy than conventional {111} and {100} crystal planes, leading to a better performance in supercapacitors.

In another comprehensive study [114], single crystalline and mesoporous nanorods, nanobelts and nanosheets Co_3O_4 samples with predominantly exposed high-energy $\{1\bar{1}0\}$ crystal

planes demonstrated excellent electrochemical properties in supercapacitors, providing higher capacitance and better rate capability than conventional cubic/octahedral Co_3O_4 nanoparticles with low-energy {100} and {111} planes. Fig. 10 shows the cyclic voltammetry (CV) curves of three different electrochemical performances of Co_3O_4 samples. Co_3O_4 nanosheets demonstrated the highest capacitance and highest rate capability. The facet-promoted electrochemical performance was not fully discovered, and was tentatively attributed to ultrathin thickness and mesoporosity for better diffusion of the electrolyte without an internal pressure and delayed effect. [114]

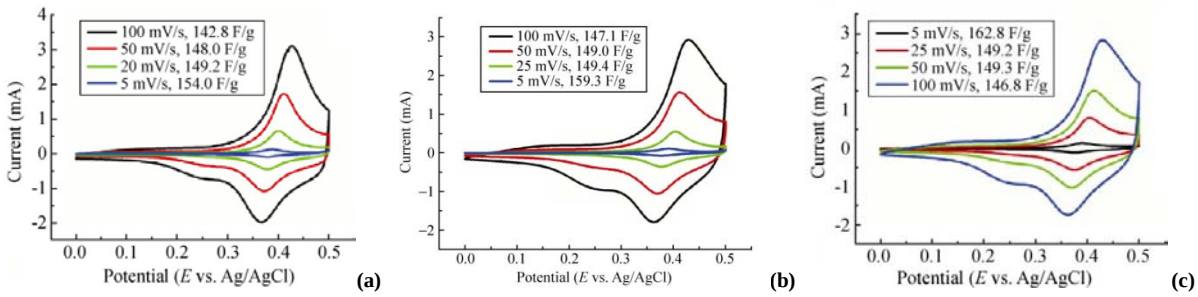

Figure 10 Cyclic voltammetry (CV) curves of Co_3O_4 nanorods (a), nanobelts (b) and nanosheets (c). Reproduced from Ref. [114] with permission from Springer.

4. Mechanism of facets-related enhancement

The effect of structure/shape/morphology on the properties of a material has long been recognized;[115, 116] however, scientific understandings at molecular level to the mechanism have not yet been fully discovered.

Shape-controlled synthesis has been achieved in the scope of novel metal nanocrystals, such as platinum,[117] gold,[118] silver,[119] etc., due to their significant applications in catalysis and the simplicity being elementary crystals. El-Sayed et al. [120] compared the activation energy and other kinetic parameters of the electron-transfer reaction between hexacyanoferrate (III) ions and thiosulfate ions in colloidal solution containing dominantly tetrahedral, cubic or spherical Pt nanoparticles as catalysts. The catalytic activities of these three nanoparticles were found to correlate with the fraction of surface atoms located on corners and edges. It was further reported that the edge and corner atoms exhibited open coordination sites that may result in

significantly different bond enthalpies, desorption energies, and adsorption geometries compared to adsorption on terrace sites.[121] Sun et al. [41] proposed that facets are closely related to the density of atomic steps and dangling bonds, which would be the origin of the enhanced catalytic activity. Xu et al.[122] reviewed the synthesis and application of noble metal nanocrystals with high-energy facets, and concluded that the high density of atomic steps, edges, and kinks would make those nanocrystals with high-energy facets more active in breaking chemical bonds than common nanocrystals.

For metal oxides, the intrinsic nature to enhanced performance of the nanocrystals with predominantly exposed facets is more complicated. As a promising photocatalyst, TiO_2 with dominant high-energy facets has been extensively studied. It was found that the presence of high-energy facets in TiO_2 improves significantly its adsorption, electric, and photocatalytic properties.[19] Cheng et al. [47] systematically summarized the unique properties of shape crystals, including (i) anisotropic corrosion, (ii) interaction dependence of adsorbates, (iii) reaction selectivity, and (iv) reduction and oxidation sites. Li et al. [43] further indicated that a cooperative mechanism of surface atomic structure (the density of undercoordinated Ti atoms) and surface electronic structure (the power of photoexcited charge carriers) is the determining factor for photoreactivity.

As for the enhanced properties of Co_3O_4 with preferential facets, no conclusive mechanism has been established. Shen et al. [54] summarized the morphology/plane-dependent catalysis of these cobalt oxides in terms of CH_4 combustion and CO oxidation. Recently Li et al. [43] also mentioned the enhanced catalytic properties of Co_3O_4 with well defined facets in methane combustion and CO oxidation. It has been evidenced that the shapes of nanocrystals would significantly influence their catalytic performances. Here we extended the investigations to catalysis and electrochemical properties of Co_3O_4 with predominantly exposed planes. (a) CO oxidation: Co^{3+} is the active site rather than Co^{2+}, so the facets with more Co^{3+} would be more active than those with Co^{2+}. Moreover, Co^{3+} sites of {011} planes is of much higher activity than {001} planes. (b) Li-ion battery and supercapacitor: Smaller size, porous structure, and favourability for electron transportation and insertion and extraction of lithium ions of one-dimensional nanostructures. The {111} facets and higher energy facets of $\{\bar{1}12\}$ would also promote the electrochemical properties. (c) Methane combustion: The surface atom arrangement of the Co_3O_4 with different planes is responsible for the different catalytic

activities. (d) Ethylene oxidation: Co^{3+} cations on the {110} planes would provide sufficient sites for ethylene oxidation, and oxygen vacancies play a key role as well. Based on above conclusive findings, it is shown that the insights of enhanced properties of Co_3O_4 with predominantly exposed facets are still yet fully understood.

Density functional theory (DFT) calculations were applied to discover the differences in bulk and surface properties (naturally occurring (110) and (111) surfaces) of spinel Co_3O_4. The magnetic structure, band gaps, density of states and possible optical-transition bands of the bulk, and structure, relaxation and stability of Co_3O_4 (110) and (111) surface were studied. Results suggested that significant differences exist between bulk and surface, and between surfaces of (100) and (111). The differences in properties are originally resulted from their different chemical compositions and different atoms arrangements.[93] Zasada et al. [123] presented periodic DFT and atomic thermodynamic studies of Co_3O_4 nanocrystals in wet environment by investigating the molecular interpretation of water adsorption equilibria. The thermal behaviour of the hydrated (110) surface was clearly different from that of (100) surface. For the (111) termination, the situation was quite similar to that observed in the case of the (110) plane. They further reported periodic DFT and HR-STEM studies of surface structure and morphology of Co_3O_4 nanocrystals.[25] The results of slab calculations enabled to evaluate the surface structure and reconstruction of the low index (100), (110) and (111) planes. The surface energies of the relaxed facets increased as 1.39 J m^{-2}(100) < 1.48 J m^{-2} (111) < 1.65 J m^{-2} (110). Fig. 11 shows selected projections of the reconstructed polyhedral shapes of the Co_3O_4 crystallites, STEM images and corresponding Fast Fourier Transform (FFT) patterns. The results clearly showed that different crystallographic planes refer to different spacing. The symmetry of the diffraction spots in the FFT patterns also strongly indicated the orientation of the observed faceted particles, allowing for univocal alignment of the predicted 3D Wulff shapes with respect to the experimental 2D images.

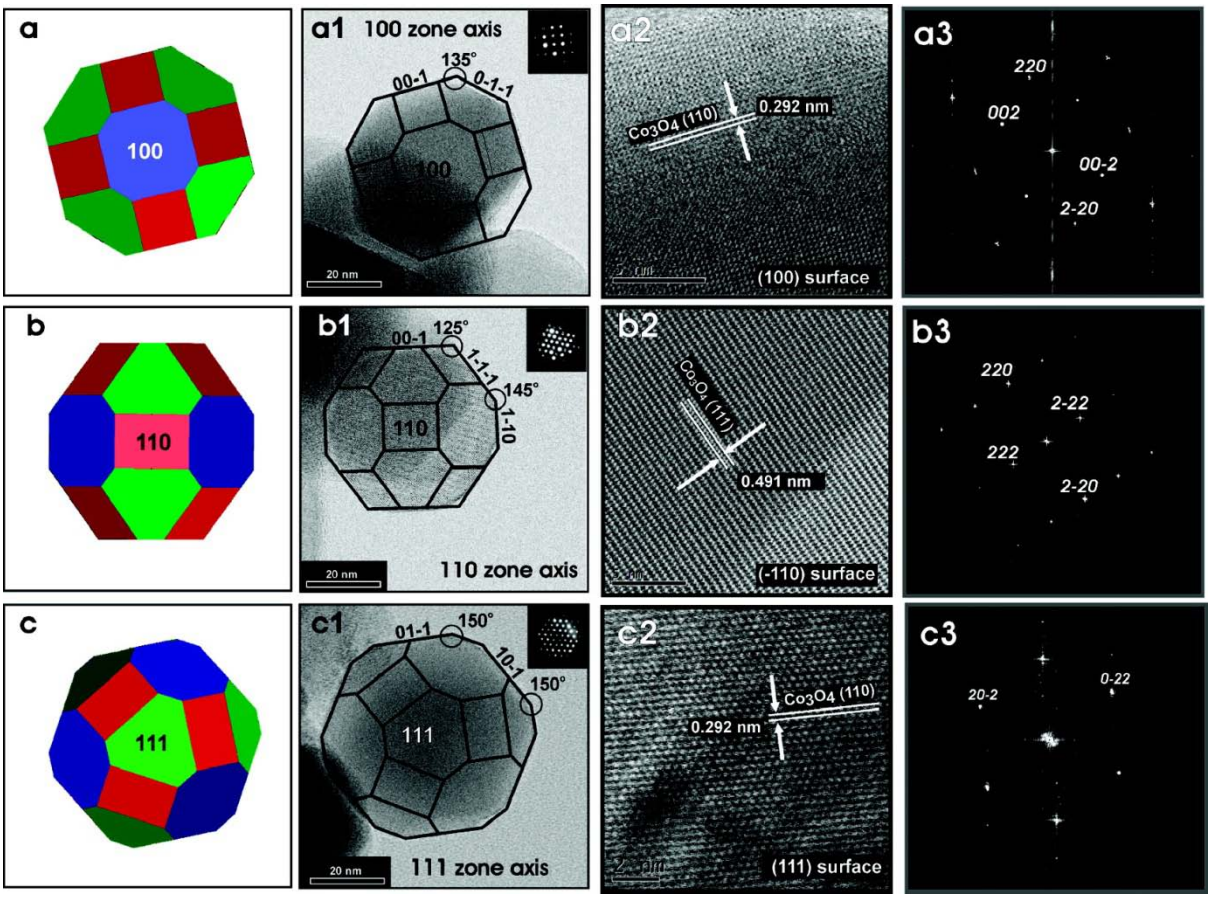

Figure 11 Thermodynamical Wulff shape (a–c) together with reconstructed STEM shapes (a1−c1) of cobalt nanocrystals viewed along the [100], [110], and [111] directions. HRTEM images of the exposed Co_3O_4 planes (a2–c2), together with the corresponding fast Fourier transform (a3–c3) indexed within the *Fm3m* space group. Reproduced from Ref. [25] with permission from RSC.

Xu et al. [26] studied the adsorption of H_2O and its effect on CO oxidation over Co_3O_4 (110) surface by DFT studies, theoretically correlating surface structure to adsorption and catalysis. H_2O was found to be adsorbed favourably at Co^{oct} sites on the surface, by O bonding with Co^{oct} sites and hydrogen bond formation between surface active oxygen atoms (O^{2f} or O^{3f}) and H. Hydrogen bonding would play a key role for H_2O adsorption at the Co^{oct} sites. H_2O adsorption at the Co^{oct} sites by hydrogen bonding to the O^{2f} sites can present an inhibition effect on CO interaction with the O^{2f} sites, and then further hinders the CO_2 formation by abstracting O^{2f} atoms to a certain extent. The results provide a valuable method for investigation on the shape-related catalysis; however, the electrochemical performances of different shape Co_3O_4 have not been investigated theoretically.

5. Conclusions and Perspectives

Nanocrystalline Co_3O_4 has demonstrated a wide range of applications in energy storage and environmental remediation. Extensive studies from world-wide researchers have evidenced that with or without capping agents, different shapes of nanosized Co_3O_4, such as sphere, cube, sheet, belt, rod, plate, tube, wire, octahedron and mesh can be successfully prepared. The crystal planes are closely related to the morphology of nanoparticles; therefore, Co_3O_4 with predominantly exposed facets can be designed and fabricated. Enhanced performances of the Co_3O_4 samples with preferential planes have been observed in many applications, such as CO oxidation, methane combustion, Li-ion battery, supercapacitor, ethylene oxidation, gas sensor, etc. The mechanism for activity enhancement varies, generally, unique structure, large surface area, abundance of Co^{3+}, oxygen vacancies, and surface atom arrangement would contribute to the enhancements of activity and selectivity. All the features mentioned above can be correlated to the crystal planes. Nevertheless, the research progress in the field of Co_3O_4 is still young compared with that of novel metal nanoparticles due to complex structure.

Therefore, in the pursuit of rational design of Co_3O_4 nanocrystals with selected facets and a better understanding of the mechanism of promoted performances in the applications, following research activities are expected to be paid more attention. (a) Theoretical studies: Thermodynamic mode of Co_3O_4 crystal growth with or without capping agents/ions has not been established. Quantum chemistry, morphological chemistry and molecular simulation are required to work together for explanation of the surface adsorption/reactions at molecular level. (b) Synthesis with manipulation at atomic level: Orientation attachment and modification need to be investigated to fabricate facet or plane with adventitious atoms, by which the effect of a single plane on the property can be discovered. (c) Emerging applications: The preferential facets and their oriented modification would not only improve the performances in conventional applications, but lead to some more novel uses. The emerging applications will also be an excellent probe reaction for studying the facet-dependent properties.

Acknowledgement

This work was financially supported by Australian Research Council Discovery Project (DP130101319) and CRC for Contamination Assessment and Remediation of the Environment (CRC-CARE, 4.1.7.11-12).

References

1. O. D. Velev and E. W. Kaler, *Adv. Mater.*, 2000, **12**, 531-534.
2. A. Navrotsky, C. C. Ma, K. Lilova and N. Birkner, *Science*, 2010, **330**, 199-201.
3. Y. H. Kim, J. S. Heo, T. H. Kim, S. Park, M. H. Yoon, J. Kim, M. S. Oh, G. R. Yi, Y. Y. Noh and S. K. Park, *Nature*, 2012, **489**, 128-U191.
4. Y. Y. Liang, M. G. Schwab, L. J. Zhi, E. Mugnaioli, U. Kolb, X. L. Feng and K. Mullen, *J. Am. Chem. Soc.*, 2010, **132**, 15030-15037.
5. F. Jiao and H. Frei, *Angew. Chem. Inte. Ed.*, 2009, **48**, 1841-1844.
6. Y. M. Dong, K. He, L. Yin and A. M. Zhang, *Nanotechnology*, 2007, **18**.
7. X. W. Xie, Y. Li, Z. Q. Liu, M. Haruta and W. J. Shen, *Nature*, 2009, **458**, 746-749.
8. H. Q. Sun, H. Y. Tian, Y. Hardjono, C. E. Buckley and S. B. Wang, *Catal. Today*, 2012, **186**, 63-68.
9. T. Zhu, J. S. Chen and X. W. Lou, *J. Mater. Chem.*, 2010, **20**, 7015-7020.
10. W. Y. Li, L. N. Xu and J. Chen, *Adv. Funct. Mater.*, 2005, **15**, 851-857.
11. Z. Wang, L. Zhou and X. W. Lou, *Adv. Mater.*, 2012, **24**, 1903-1911.
12. J. A. Koza, Z. He, A. S. Miller and J. A. Switzer, *Chem. Mater.*, 2012, **24**, 3567-3573.
13. S. Fukuzumi, Y. Yamada, T. Suenobu, K. Ohkubo and H. Kotani, *Energy Environ. Sci.*, 2011, **4**, 2754-2766.
14. A. M. Cao, J. S. Hu, H. P. Liang, W. G. Song, L. J. Wan, X. L. He, X. G. Gao and S. H. Xia, *J. Phys. Chem. B*, 2006, **110**, 15858-15863.
15. L. Fu, Z. M. Liu, Y. Q. Liu, B. X. Han, P. G. Hu, L. C. Cao and D. B. Zhu, *Adv. Mater.*, 2005, **17**, 217-218.
16. G. X. Wang, H. Liu, J. Horvat, B. Wang, S. Z. Qiao, J. Park and H. Ahn, *Chem.-A Europ. J.*, 2010, **16**, 11020-11027.
17. R. Shi, G. Chen, W. Ma, D. Zhang, G. Qiu and X. Liu, *Dalt. Transact.*, 2012, **41**, 5981-5987.
18. Z. Y. Jiang, Q. Kuang, Z. X. Xie and L. S. Zheng, *Adv. Funct. Mater.*, 2010, **20**, 3634-3645.
19. S. W. Liu, J. G. Yu and M. Jaroniec, *Chem. Mater.*, 2011, **23**, 4085-4093.
20. J. Feng and H. C. Zeng, *Chem. Mater.*, 2003, **15**, 2829-2835.
21. Y. Ding, L. Xu, C. Chen, X. Shen and S. L. Suib, *J. Phys. Chem. C*, 2008, **112**, 8177-8183.
22. T. He, D. R. Chen and X. L. Jiao, *Chem. Mater.*, 2004, **16**, 737-743.
23. S. Xiong, C. Yuan, M. Zhang, B. Xi and Y. Qian, *Chem.-A Europ. J.*, 2009, **15**, 5320-5326.
24. L. Hu, Q. Peng and Y. Li, *J. Am. Chem. Soc.*, 2008, **130**, 16136-16137.
25. F. Teng, M. D. Chen, N. Li, X. Hua, J. Wang, Q. Y. Zhang, Y. Wang, D. D. Meng and G. Q. Li, *RSC Adv.*, 2013, **3**, 743-751.

26. B. Meng, Z. B. Zhao, X. Z. Wang, J. J. Liang and J. S. Qiu, *Appl. Catal. B*, 2013, **129**, 491-500.
27. Y. G. Zhang, Y. C. Chen, J. H. Zhou, T. Wang and Y. G. Zhao, *Solid State Commun.*, 2009, **149**, 585-588.
28. G. M. Bai, H. X. Dai, J. G. Deng, Y. X. Liu, F. Wang, Z. X. Zhao, W. G. Qiu and C. T. Au, *Appl. Catal. A*, 2013, **450**, 42-49.
29. G. X. Tong, J. G. Guan and Q. J. Zhang, *Adv. Funct. Mater.*, 2013, **23**, 2406-2414.
30. J. Yang, H. Hyodo, K. Kimura and T. Sasaki, *Nanotechnology*, 2010, **21**.
31. Y. S. Luo, J. S. Luo, W. W. Zhou, X. Y. Qi, H. Zhang, D. Y. W. Yu, C. M. Li, H. J. Fan and T. Yu, *J. Mater. Chem. A*, 2013, **1**, 273-281.
32. H. M. Du, L. F. Jiao, Q. H. Wang, J. Q. Yang, L. J. Guo, Y. C. Si, Y. J. Wang and H. T. Yuan, *Nano Res.*, 2013, **6**, 87-98.
33. C. Z. Yuan, L. Yang, L. R. Hou, L. F. Shen, X. G. Zhang and X. W. Lou, *Energy Environ. Sci.*, 2012, **5**, 7883-7887.
34. Q. Hao, M. H. Li, S. Z. Jia, X. Y. Zhao and C. X. Xu, *Rsc Adv.*, 2013, **3**, 7850-7854.
35. Y. Wang, H. J. Zhang, J. Wei, C. C. Wong, J. Lin and A. Borgna, *Energy Environ. Sci.*, 2011, **4**, 1845-1854.
36. G. L. Xu, J. T. Li, L. Huang, W. F. Lin and S. G. Sun, *Nano Energy*, 2013, **2**, 394-402.
37. J. Liu, H. Xia, L. Lu and D. Xue, *J. Mater. Chem.*, 2010, **20**, 1506-1510.
38. Y. Q. Wang, C. M. Yang, W. Schmidt, B. Spliethoff, E. Bill and F. Schuth, *Adv. Mater.*, 2005, **17**, 53-+.
39. Y. Sun, P. Lv, J. Y. Yang, L. He, J. C. Nie, X. W. Liu and Y. D. Li, *Chem. Commun.*, 2011, **47**, 11279-11281.
40. Q. Yan, X. Li, Q. Zhao and G. Chen, *J. Hazard. Mater.*, 2012, **209**, 385-391.
41. N. Tian, Z. Y. Zhou, S. G. Sun, Y. Ding and Z. L. Wang, *Science*, 2007, **316**, 732-735.
42. I. Lee, F. Delbecq, R. Morales, M. A. Albiter and F. Zaera, *Nat. Mater.*, 2009, **8**, 132-138.
43. K. B. Zhou and Y. D. Li, *Angew. Chem. Inter. Ed.* 2012, **51**, 602-613.
44. M. Chen, B. H. Wu, J. Yang and N. F. Zheng, *Adv. Mater.*, 2012, **24**, 862-879.
45. W. C. Huang, L. M. Lyu, Y. C. Yang and M. H. Huang, *J. Am. Chem. Soc.*, 2012, **134**, 1261-1267.
46. Z. Y. Zhou, N. Tian, J. T. Li, I. Broadwell and S. G. Sun, *Chem. Soc. Rev.*, 2011, **40**, 4167-4185.
47. G. Liu, J. C. Yu, G. Q. Lu and H. M. Cheng, *Chem. Commun.*, 2011, **47**, 6763-6783.
48. C. Z. Wen, H. B. Jiang, S. Z. Qiao, H. G. Yang and G. Q. Lu, *J. Mater. Chem.*, 2011, **21**, 7052-7061.
49. H. B. Jiang, Q. A. Cuan, C. Z. Wen, J. Xing, D. Wu, X. Q. Gong, C. Z. Li and H. G. Yang, *Angew. Chem. Inter. Ed.*, 2011, **50**, 3764-3768.
50. W. Q. Fang, X. H. Yang, H. J. Zhu, Z. Li, H. J. Zhao, X. D. Yao and H. G. Yang, *J. Mater. Chem.*, 2012, **22**, 22082-22089.
51. J. Strunk, K. Kahler, X. Y. Xia and M. Muhler, *Surf. Sci.*, 2009, **603**, 1776-1783.
52. J. S. Chen, L. A. Archer and X. W. Lou, *J. Mater. Chem.*, 2011, **21**, 9912-9924.
53. Z. B. Zhuang, Q. Peng and Y. D. Li, *Chem. Soc. Rev.*, 2011, **40**, 5492-5513.

54. X. Xie and W. Shen, *Nanoscale*, 2009, **1**, 50-60.
55. S. Y. Lian, E. B. Wang, L. Gao and L. Xu, *Mater. Lett.*, 2007, **61**, 3893-3896.
56. X. H. Liu, G. Z. Qiu and X. G. Li, *Nanotechnology*, 2005, **16**, 3035-3040.
57. J. Yang and T. Sasaki, *Cryst. Growth Des.*, 2010, **10**, 1233-1236.
58. Y. H. Teng, Y. Kusano, M. Azuma, M. Haruta and Y. Shimakawa, *Catal. Sci. Technol.*, 2011, **1**, 920-922.
59. X. L. Xiao, X. F. Liu, H. Zhao, D. F. Chen, F. Z. Liu, J. H. Xiang, Z. B. Hu and Y. D. Li, *Adv. Mater.*, 2012, **24**, 5762-5766.
60. W. M. Mei, J. Huang, L. P. Zhu, Z. Z. Ye, Y. J. Mai and J. P. Tu, *J. Mater. Chem.*, 2012, **22**, 9315-9321.
61. S. Sharma, N. Garg, K. V. Ramanujachary, S. E. Lofland and A. K. Ganguli, *Cryst. Growth Des.*, 2012, **12**, 4202-4210.
62. Y. Li, J. Zhao, Y. Dan, D. Ma, Y. Zhao, S. Hou, H. Lin and Z. Wang, *Chem. Engin. J.*, 2011, **166**, 428-434.
63. Y. Sun, R. Xu, J. Y. Yang, L. He, J. C. Nie, R. F. Dou, W. Zhou and L. Guo, *Nanotechnology*, 2010, **21**.
64. X. Wang, H. Guan, S. Chen, H. Li, T. Zhai, D. Tang, Y. Bando and D. Golberg, *Chem. Commun.*, 2011, **47**, 12280-12282.
65. T. He, D. R. Chen, X. L. Jiao, Y. Y. Xu and Y. X. Gu, *Langmuir*, 2004, **20**, 8404-8408.
66. X. Wang, X. L. Wu, Y. G. Guo, Y. T. Zhong, X. Q. Cao, Y. Ma and J. N. Yao, *Adv. Funct. Mater.*, 2010, **20**, 1680-1686.
67. X. Guo, W. Xu, S. Li, Y. Liu, M. Li, X. Qu, C. Mao, X. Cui and C. Chen, *Nanotechnology*, 2012, **23**.
68. M. Wang, L. Zeng and Q. Chen, *Dalt. Transact.*, 2011, **40**, 597-601.
69. X. C. Song, X. Wang, Y. F. Zheng, R. Ma and H. Y. Yin, *J. Nanopart. Res.*, 2011, **13**, 1319-1324.
70. H. Liang, J. M. Raitano, L. Zhang and S.-W. Chan, *Chem. Commun.*, 2009, 7569-7571.
71. L. Chen, J. Hu, R. Richards, S. Prikhodko and S. Kodambaka, *Nanoscale*, 2010, **2**, 1657-1660.
72. L. Hu, K. Sun, Q. Peng, B. Xu and Y. Li, *Nano Res.*, 2010, **3**, 363-368.
73. L. Tian, H. L. Zou, J. X. Fu, X. F. Yang, Y. Wang, H. L. Guo, X. H. Fu, C. L. Liang, M. M. Wu, P. K. Shen and Q. M. Gao, *Adv. Funct. Mater.*, 2010, **20**, 617-623.
74. X. F. Ke, J. M. Cao, M. B. Zheng, Y. P. Chen, J. S. Liu and G. B. Ji, *Mater. Lett.*, 2007, **61**, 3901-3903.
75. J. Q. Wang, G. D. Du, R. Zeng, B. Niu, Z. X. Chen, Z. P. Guo and S. X. Dou, *Electrochim. Acta*, 2010, **55**, 4805-4811.
76. X. W. Lou, D. Deng, J. Y. Lee, J. Feng and L. A. Archer, *Adv. Mater.*, 2008, **20**, 258-259.
77. Z. Y. Fei, S. C. He, L. Li, W. J. Ji and C. T. Au, *Chem. Commun.*, 2012, **48**, 853-855.
78. Z. Dong, Y. Y. Fu, Q. Han, Y. Y. Xu and H. Zhang, *J. Phys. Chem. C*, 2007, **111**, 18475-18478.

79. X. H. Xia, J. P. Tu, Y. Q. Zhang, Y. J. Mai, X. L. Wang, C. D. Gu and X. B. Zhao, *RSC Adv.*, 2012, **2**, 1835-1841.
80. P. Zhang, G.-X. Hu, S.-J. Bao, J. Guo, C. Lei, C.-J. Cai, D.-Z. Jia and R.-Y. Wang, *Mater. Lett.*, 2012, **83**, 195-197.
81. J. W. Saalfrank and W. F. Maier, *Angew. Chem. Inter. Ed.*, 2004, **43**, 2028-2031.
82. J. Jansson, A. E. C. Palmqvist, E. Fridell, M. Skoglundh, L. Osterlund, P. Thormahlen and V. Langer, *J. Catal.*, 2002, **211**, 387-397.
83. M. Haruta, S. Tsubota, T. Kobayashi, H. Kageyama, M. J. Genet and B. Delmon, *J. Catal.*, 1993, **144**, 175-192.
84. M. Date, M. Okumura, S. Tsubota and M. Haruta, *Angew. Chem. Inter. Ed.*, 2004, **43**, 2129-2132.
85. F. Romero-Sarria, M. I. Dominguez, M. A. Centeno and J. A. Odriozola, *Appl. Catal. B*, 2011, **107**, 268-273.
86. S. Wendt, M. Knapp and H. Over, *J. Am. Chem. Soc.*, 2004, **126**, 1537-1541.
87. L. Zang and H. Kisch, *Angew. Chem. Inter. Ed.*, 2000, **39**, 3921-+.
88. J. Jansson, *J. Catal.*, 2000, **194**, 55-60.
89. C. J. Jia, M. Schwickardi, C. Weidenthaler, W. Schmidt, S. Korhonen, B. M. Weckhuysen and F. Schuth, *J. Am. Chem. Soc.*, 2011, **133**, 11279-11288.
90. A. D. Pandey, C. J. Jia, W. Schmidt, M. Leoni, M. Schwickardi, F. Schuth and C. Weidenthaler, *J. Phys. Chem. C*, 2012, **116**, 19405-19412.
91. H. F. Wang, R. Kavanagh, Y. L. Guo, Y. Guo, G. Z. Lu and P. Hu, *J. Catal.*, 2012, **296**, 110-119.
92. P. Broqvist, I. Panas and H. Persson, *J. Catal.*, 2002, **210**, 198-206.
93. X. L. Xu, Z. H. Chen, Y. Li, W. K. Chen and J. Q. Li, *Surf. Sci.*, 2009, **603**, 653-658.
94. X. Tang, J. Li and J. Hao, *Mater. Res. Bull.*, 2008, **43**, 2912-2918.
95. C. Y. Ma, Z. Mu, J. J. Li, Y. G. Jin, J. Cheng, G. Q. Lu, Z. P. Hao and S. Z. Qiao, *J. Am. Chem. Soc.*, 2010, **132**, 2608-2613.
96. W. J. Xue, Y. F. Wang, P. Li, Z.-T. Liu, Z. P. Hao and C. Y. Ma, *Catal. Commun.*, 2011, **12**, 1265-1268.
97. X. Wang, L. Ding, Z. Zhao, W. Xu, B. Meng and J. Qiu, *Catal. Today*, 2011, **175**, 509-514.
98. J. M. Tarascon and M. Armand, *Nature*, 2001, **414**, 359-367.
99. Y. Wang and G. Z. Cao, *Adv. Mater.*, 2008, **20**, 2251-2269.
100. B. Scrosati and J. Garche, *J. Power Sour.*, 2010, **195**, 2419-2430.
101. P. Poizot, S. Laruelle, S. Grugeon, L. Dupont and J. M. Tarascon, *Nature*, 2000, **407**, 496-499.
102. J. S. Chen, T. Zhu, Q. H. Hu, J. Gao, F. Su, S. Z. Qiao and X. W. Lou, *ACS Appl. Mater. Interf.*, 2010, **2**, 3628-3635.
103. C. C. Li, X. M. Yin, Q. H. Li, L. B. Chen and T. H. Wang, *Chem.-A Europ. J.*, 2011, **17**, 1596-1604.
104. M. S. Islam, D. J. Driscoll, C. A. J. Fisher and P. R. Slater, *Chem. Mater.*, 2005, **17**, 5085-5092.

105. G. Z. Wei, X. Lu, F. S. Ke, L. Huang, J. T. Li, Z. X. Wang, Z. Y. Zhou and S. G. Sun, *Adv. Mater.*, 2010, **22**, 4364-4365.
106. X. L. Xiao, X. F. Liu, L. Wang, H. Zhao, Z. B. Hu, X. M. He and Y. D. Li, *Nano Res.*, 2012, **5**, 395-401.
107. G. B. Zhong, Y. Y. Wang, X. J. Zhao, Q. S. Wang, Y. Yu and C. H. Chen, *J. Power Sour.*, 2012, **216**, 368-375.
108. H. Sclar, O. Haik, T. Menachem, J. Grinblat, N. Leifer, A. Meitav, S. Luski and D. Aurbach, *J. Electrochem. Soc.*, 2012, **159**, A228-A237.
109. X. Li, G. L. Xu, F. Fu, Z. Lin, Q. Wang, L. Huang, J. T. Li and S. G. Sun, *Electrochim. Acta*, 2013, **96**, 134-140.
110. L. Yang, S. Cheng, Y. Ding, X. Zhu, Z. L. Wang and M. Liu, *Nano Lett.*, 2012, **12**, 321-325.
111. P. Simon and Y. Gogotsi, *Nat. Mater.*, 2008, **7**, 845-854.
112. D. W. Wang, Q. H. Wang and T. M. Wang, *Inorg. Chem.*, 2011, **50**, 6482-6492.
113. T. Brezesinski, J. Wang, R. Senter, K. Brezesinski, B. Dunn and S. H. Tolbert, *ACS Nano*, 2010, **4**, 967-977.
114. Y. Wang, Z. Zhong, Y. Chen, C. T. Ng and J. Lin, *Nano Res.*, 2011, **4**, 695-704.
115. G. A. Somorjai, *Catal. Rev.*, 1972, **7**, 87-&.
116. M. S. Chen and D. W. Goodman, *Science*, 2004, **306**, 252-255.
117. T. S. Ahmadi, Z. L. Wang, T. C. Green, A. Henglein and M. A. ElSayed, *Science*, 1996, **272**, 1924-1926.
118. M. Grzelczak, J. Perez-Juste, P. Mulvaney and L. M. Liz-Marzan, *Chem. Soc. Rev.*, 2008, **37**, 1783-1791.
119. Y. G. Sun and Y. N. Xia, *Science*, 2002, **298**, 2176-2179.
120. R. Narayanan and M. A. El-Sayed, *Nano Lett.*, 2004, **4**, 1343-1348.
121. K. M. Bratlie, H. Lee, K. Komvopoulos, P. D. Yang and G. A. Somorjai, *Nano Lett.*, 2007, **7**, 3097-3101.
122. L. Zhang, W. Niu and G. Xu, *Nano Today*, 2012, **7**, 586-605.
123. F. Zasada, W. Piskorz, S. Cristol, J. F. Paul, A. Kotarba and Z. Sojka, *J. Phys. Chem. C*, 2010, **114**, 22245-22253.